Hydantoins and Mercaptoimidazoles:

Vibrational Spectroscopy as a Probe of Structure and Reactivity in Different Environments, from the Isolated Molecule to Polymorphs

Rui Fausto,[1] Gulce O. Ildiz,[1,2] Elisa M. Brás[1] and Bernardo A. Nogueira[1]

[1] *CQC, Department of Chemistry, University of Coimbra, P-3004-535 Coimbra, Portugal*
[2] *Faculty of Sciences and Letters, Department of Physics, Istanbul Kultur University, Ataköy Campus, Bakirköy 34156, Istanbul, Turkey*

Abstract: In this Chapter, we highlight the power of vibrational spectroscopy as central technique to investigate the structure and reactivity of two relevant families of nitrogen-containing heterocyclic molecules: hydantoins, and mercaptoimidazoles. Infrared spectroscopy is used in connection with the matrix isolation technique to investigate the structures of the isolated molecules and their photochemistry, while both infrared and Raman spectroscopies, supplemented by thermodynamics, microscopy and diffraction techniques, are used to investigate neat condensed phases of the compounds and transitions between these phases. The experimental studies are supported by extensive computational studies, which include several approaches for detailed analysis of the electron density.

1. Introduction

Vibrational spectroscopy has long been recognized as a powerful technique for investigation of structure and reactivity of chemical systems in different conditions. The technological progresses achieved in the last decades in instrumentation, together with the development of new, powerful variants of the fundamental vibrational spectroscopy methods and sampling techniques, allowed the modern vibrational spectroscopies to reach an unprecedented level of sophistication. Moreover, the availability of fast computers and efficient software for data collection and analysis, as well as for prediction of vibrational spectra, has also strongly contributed to the success of vibrational spectroscopy in the present days. One has nowadays available experimental data of superior quality, and their interpretation can be ground in solid theoretical foundations, facilitated by the comparison of experimental and calculated spectra, and helped by use of modern, effective data post-processing methods, including multivariate statistical based procedures.

If *per se* vibrational spectroscopy is already an authoritative technique for structure and reactivity evaluation, when used simultaneously with other experimental methods it strongly increases its predictive and interpretative power. Among these, X-ray diffraction (XRD), allowing access to details of the structure of crystalline materials, and thermodynamic methods (such as differential scanning calorimetry; DSC), providing information on phase transition properties, deserve here to be mentioned. Vibrational spectroscopy can use structural information obtained from XRD and extract detailed information on several important properties of the crystalline materials not easy accessible (or not accessible at all) to X-ray diffraction methods, in particular those that are related with hydrogen atoms, which are weak X-ray scatters. Hydrogen bonding,

above all, has been a relevant subject for which vibrational spectroscopy has proved to be a superior investigation method. On the other way, vibrational spectroscopy, being a molecule-based technique, magnifies the interpretative capabilities of the thermodynamic approaches on differentiating and characterizing structurally different phases of a compound, and interpreting phase transition data at a molecular level.

For studies on isolated molecules, matrix isolation vibrational spectroscopy (in particular matrix isolation infrared spectroscopy) has emerging as a very powerful and elegant method, overcoming some of the difficulties of gas phase spectroscopy, such as the complexity of the spectra resulting from rotational structure, extensive anharmonic contributions, and the need for the compound under study to have a substantial vapor pressure in order to acquire good quality spectra.

Matrix isolation is a technique where molecules are trapped from the gas phase in an environment of solidified inert gases at temperatures close to absolute zero. The method was first developed almost simultaneously by the groups of Pimentel, at Berkeley (USA), and Porter, at Cambridge (UK) [1,2], and had its name coined in the historical paper by Pimentel, Whittle and Dows *"Matrix Isolation Method for the Experimental Study of Unstable Species"*, a single-page paper which appeared in the Journal of Chemical Physics, in 1954 [1].

Though matrix isolation was invented as a tool for study reactive species, the method has also many advantages over other techniques for the study of stable molecules, and has been used extensively for this purpose too. The main advantages of the method can be attributed to the very low work temperature, virtual absence of intermolecular interactions between the molecules under investigation, and rigidity and chemical inertness of the matrix medium. Because inert gases are generally used as matrix host, solute-solvent interactions can be neglected for most of the practical applications. On the other hand, molecular diffusion and rotation are inhibited (except in the case of very small molecules), allowing registering of pure vibrational spectra, which can be easily compared with theoretically predicted spectroscopic data (that are usually obtained for molecules *in vacuo*). Also, hot vibrational transitions as well as subtractive combination tones are suppressed, since excited vibrational states are depopulated at the low work temperatures typical of the matrix isolation experiments, introducing an additional simplification in the spectra and contributing to their increased resolution.

Another interesting feature of matrix isolation, this time particularly useful for reactivity studies (in particular in photochemistry), results from the fact that isolated molecules in matrices are cage confined. Thus, if fragmentation of a matrix-isolated species takes place, for example in result of photoexcitation, in most of the times the obtained fragments stay in the matrix cage where they were formed. Thus, no subsequent cross-reactions involving species resulting from fragmentation of different reactant molecules can occur, strongly reducing the number of possible products in comparison with gas phase or solution studies, and open the gate for a detailed study of the mechanisms of unimolecular photochemically-induced processes.

In addition to the above-mentioned advantages, standard matrix isolation setups can be also used, without any modification, for preparation of samples of a solid pristine compound, by the sole condensation of its vapor. This method of sample preparation in general leads to producing of amorphous solids that can then be submitted to a controlled temperature program to induce *in situ* crystallization, which can be spectroscopically followed. The temperature program can be chosen to mimic a temperature program used,

for example, in a DSC experiment, so that spectroscopic data can be directly compared with thermodynamic information.

In the studies described in the present Chapter, matrix isolation infrared spectroscopy has been used to investigate the structures of the isolated molecules of the targeted compounds and their photochemistry. The neat condensed phases, and phase transitions, have been investigated by infrared and Raman spectroscopies, supplemented by DSC, polarized-light thermomicroscopy (PLTM), and XRD. Computational studies, including use of several approaches for detailed analysis of the electron density of the investigated molecules, were used to help interpreting the experimental data. On the whole, it is our aim to highlight here the power of vibrational spectroscopy as central technique to investigate the structure and reactivity of two relevant families of nitrogen-containing heterocyclic molecules: hydantoins and mercaptoimidazoles.

2. Structures and infrared spectra of the isolated molecules

2.1. *Mercaptoimidazoles*

Mercaptoimidazoles constitute an important family of nitrogen-containing heterocyclic molecules that has been shown to present antioxidant properties towards several oxygen-derived toxic species. The mercaptoimidazole moiety is present in natural antioxidant compounds such as ergothioneine or ovothiol [3-6]. Mercaptoimidazoles are also similar compounds to thiouracil, a relevant anti-thyroid drug that was used for the first time in 1943 as therapy of Graves' disease [7], and that is still in use nowadays.

An interesting property of this type of compounds is that they may undergo slow oxidation to the disulfide dimeric form in acidic media [8]. In turn, structurally appropriate disulfides may undergo homolytic S-S bond photodissociation into a pair of radicals exhibiting suitable magnetic and/or optical properties to act as photoswitches [9,10].

The molecules studied in our laboratory were 2-thiobenzimidazole (**TBI**), 1-methyl-2-thioimidazole (**MTI**) and 1-methyl-2-thiobenzimidazole (**MTBI**). All these molecules can exist in two tautomeric forms, thione and thiol, whose structures are represented in Figure 1. DFT(B3LYP)/6-311++G(d,p) calculations demonstrated that, for all molecules, the thione tautomer is more stable than the thiol form [11,12]. The relative energy difference between the tautomers increases in the order **MTI** < **TBI** < **MTBI** (38.8, 44.6 and 49.8 kJ mol^{-1}, respectively), indicating that the presence of both benzo and methyl substituents stabilizes the thione tautomer. In the thiol tautomer, the SH group points towards the imine ring nitrogen atom (see Figure 1), both to minimize repulsions between the sulphidryl hydrogen atom and the ortho hydrogen atom or methyl substituent and to maximize the attractive interaction between the nearly anti-parallel bond dipoles associated with the SH and C=N ring bonds.

In practical terms, the heavy atom skeleton of the two tautomers of all studied molecules is planar. In the case of the thione tautomers, the heavy atom skeleton planar structures correspond to true minima on the investigated potential energy surfaces. For thiol forms, the planar geometry is also a minimum energy structure for **TBI**, while for the methyl substituted molecules (**MTI**, **MTBI**) the calculations predict two slightly non-planar equivalent-by-symmetry minima, with N=C–S–H dihedral angles of a few degrees. However, these forms are separated from each other by a very low energy barrier (below

0.1 kJ mol^{-1}), which stays below the zero-point vibrational level of these structures. Under these circumstances, the heavy atom skeleton planar geometry corresponds also to the most probable structure for the two molecules in the ground vibrational state, thus being the one relevant in practical terms.

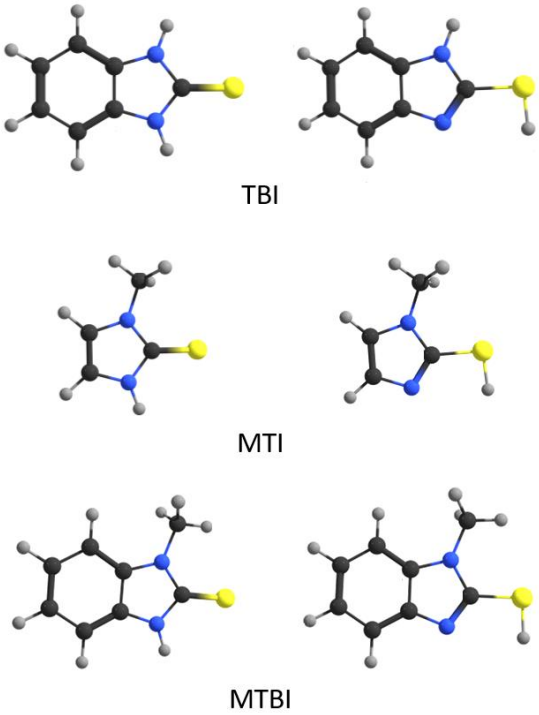

Fig. 1. Structures of **TBI**, **MTI** and **MTBI** tautomeric forms (thione: *left*; thiol: *right*).

An interesting distinct structural feature in the two methyl substituted molecules is the orientation of the methyl group (see Figure 1). In **MTI**, the methyl group is oriented in such a way that the methyl hydrogen atom placed in the plane of the heavy-atom skeleton of the molecule points away from the sulfur substituent, in order to minimize the methyl/S steric repulsions. This is true for both thione and thiol tautomers. On the other hand, in **MTBI** the in-plane methyl hydrogen atom points towards the sulfur substituent in both tautomeric forms, because in this case the presence of the benzo-substituent introduces a stronger steric/electrostatic repulsion between the methyl group and the closest located phenyl hydrogen atom. Such interaction can in fact be expected to attain its maximum importance for an orientation of the methyl group identical to that found in **MTI**.

More important is the conclusion, extracted from the structural data obtained for all molecules, that no intramolecular hydrogen bond exists in any of the tautomers. In fact, the ∢N–H···S and ∢S–H···N angles in the thione and thiol tautomers, respectively, are in the range 67-82º, *i.e.*, they are considerably smaller than the commonly accepted minimum value for a ∢D–H···A (D, donor; A, acceptor) angle allowing the establishment of a hydrogen bond (~110º [13]). As it will be shown in the Section 3.1, this structural feature is of extreme importance in determining the mechanism of unimolecular photo-tautomerization in these molecules.

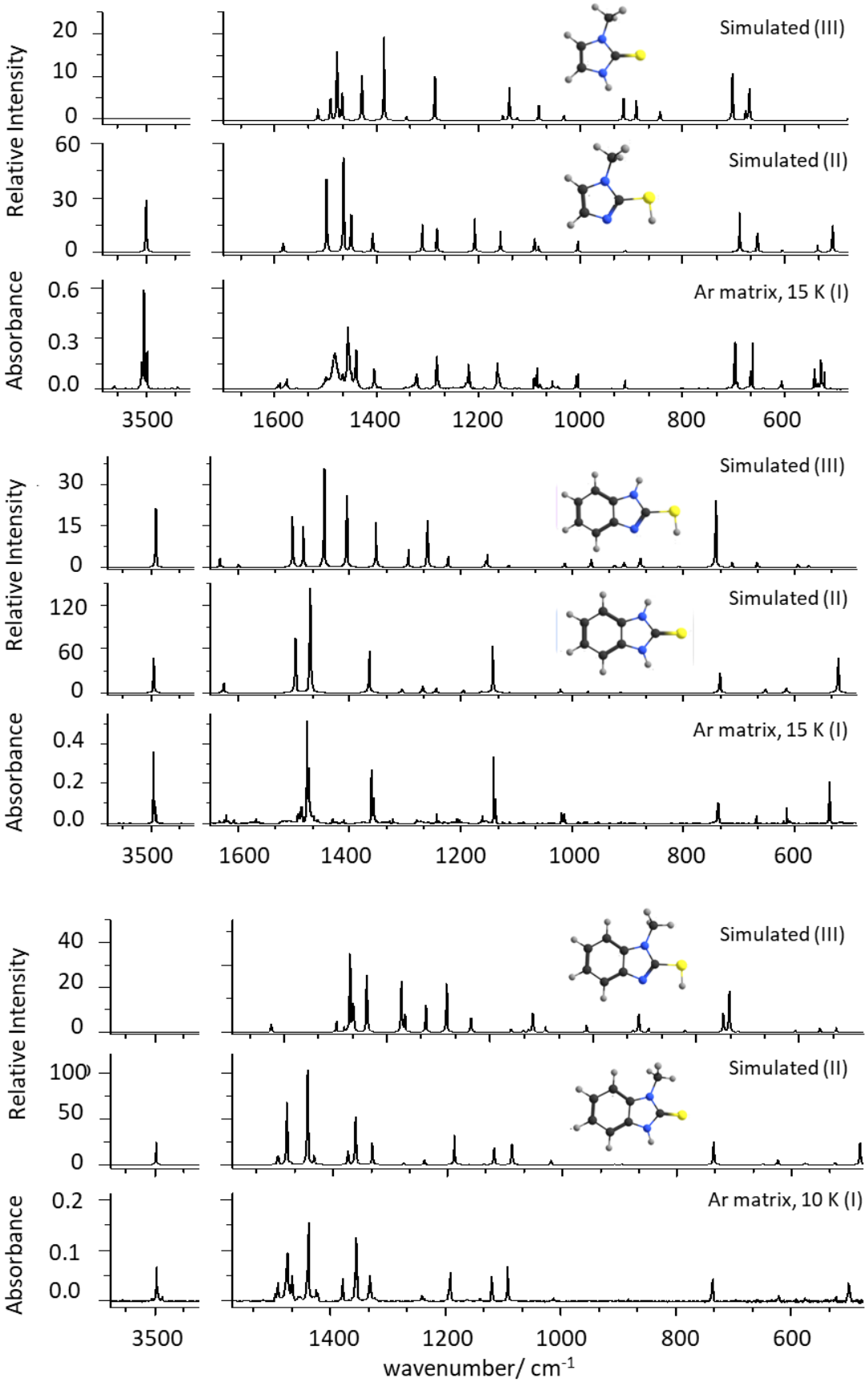

Fig. 2. Experimental infrared spectrum of **MTI** (*top*), **TBI** (*middle*) and **MTBI** (*bottom*) isolated in an argon matrix (I), compared with the B3LYP/6-311++G(d,p) calculated spectra of thione and thiol tautomers (II and III, respectively).

The infrared spectra of the matrix-isolated compounds are shown in Figure 2, where they can be compared with the theoretically predicted spectra for the two tautomers. The results are clear regarding the sole presence in the matrices of the thione tautomer. This result allows us also to conclude that no tautomerization takes place upon sublimation of the compounds, and that the thione form, which was initially present in the crystals [14-16], was kept upon the phase transition.

The excellent agreement between the calculated and experimental data facilitated the assignment of the bands, which can be found in Refs. [12,13]. The two striking observations are: *(i)* the extensive site splitting and broadening observed for the bands assigned to vibrations with dominant contributions of the NH modes (in particular the bending and rocking modes), which demonstrates the involvement of the NH moieties in specific interactions with the host matrix atoms and reflects in the observed high-sensitivity of the vibrations of the NH groups to local environment, and *(ii)* for the methyl substituted compounds, also the splitting and relative broadening of the bands associated with the bending vibrations of the methyl group, which points to a partially free rotation of this group even in the matrix media, thus implying a large amplitude methyl torsional vibration that, in turn, leads to an increased dispersion of the vibrational levels associated with the bending modes. In consonance with the spectroscopically suggested appreciable conformational freedom of the methyl groups, the B3LYP/6-311++G(d,p) calculated methyl internal rotation barriers for **MTI** and **MTBI** amount only to 1.2 and 2.7 kJ mol^{-1}, respectively [12,13].

2.2. *Hydantoins*

Hydantoins are heterocyclic compounds that derive from imidazolidine. They exhibit relevant physiological activities, for example as anticonvulsive, antiepileptic, anti-inflammatory and anti-cancer drugs [17-22], and have also been suggested as potential therapeutic agents for the treatment of HIV-1 [23,24].

Like mercaptoimidazoles, hydantoins may also exhibit tautomerism, and tautomeric forms of hydantoins bearing either one or two OH moieties may also be conceivable to exist. Taking the di-keto most stable tautomer as reference, these tautomers can be viewed as resulting from migration of the lactam hydrogen atoms to the carbonyl oxygen atoms. However, these tautomers have been shown to be higher in energy than the most stable tautomer by at least 70 kJ mol^{-1} [25], and have never been observed experimentally for the simplest members of the family.

In our studies on hydantoins [26-30], we have considered both 1-methyl and 5-methyl substituted hydantoins (**1MH**, **5MH**), and 5-acetic acid hydantoin (**AAH**), besides the parent, unsubstituted hydantoin (**H**) (Figure 3). Those studies allowed us to establish the basic structural properties of the hydantoin moiety. It could be concluded, for example, that the hydantoin ring tends to assume a planar (or quasi-planar) geometry, sharing common geometrical and electronic features in all investigated compounds. To mention just the most important ones: *(i)* the relative lengths of the two distinct C=O bonds in the ring are dictated by the degree of π electronic delocalization from the nitrogen atoms, being longer when the C=O fragment is connected to two nitrogen atoms than when connected to a single nitrogen; *(ii)* the internal angles of the ring with a nitrogen atom in the apex are much larger (around 113º) than those with carbon atoms in the apex (~101-106º), due to different *s–p* compositions of the hybrid orbitals of the N and C atoms used

to make the ring bonds; *(iii)* the π charge of the oxygen atom of the carbonyl group connected to two nitrogen atoms is more negative than that of the oxygen atom of the second carbonyl group (connected to a single nitrogen atom), in agreement with its longer bond length and involvement in a more extended π mesomerism; and *(iv)* the *σ* charges of the two oxygen atoms are considerably less negative than the corresponding *π* charges and have opposite relative values, showing that a larger *π* bond polarization towards the oxygen atom leads to reduce the trend for the associated *σ* bond to be polarized in the same direction. These structural characteristics have relevant consequences for the reactivity of the hydantoin moiety, as it will be pointed out in Section 3.2.

The parent hydantoin, as well as its studied methyl derivatives (**1MH**, **5MH**) have no conformational flexibility, being, by that reason, quite rigid structurally. On the other hand, **AAH** bears a conformationally flexible substituent, with 3 different conformationally relevant degrees of freedom, and has 13 different conformers: 6 forms bearing a *cis* carboxylic group (O=C–O–H dihedral of ~0º), and 7 possessing this group in the *trans* configuration (~180º). The most stable conformer of **AAH** is shown in Figure 3, being a *cis* carboxylic acid form. The remaining *cis* carboxylic acid conformers have relative energies within 17 kJ mol^{-1} [B3LYP/6-311++G(d,p) calculated values], while all *trans* carboxylic acid conformers have relative energies of at least 19 kJ mol^{-1}, with the highest energy conformer (see Figure 3) having a relative energy of about 40 kJ mol^{-1}.

The electronic structure of the studied hydantoins was investigated by several methods of electron density analysis, starting with the simple picture provided by atomic charges π/σ partition, and going through Natural Bond Orbital (NBO) and Atoms in Molecules (AIM) analyses. All these analyses were found to be consistent with the usual representation of the structure of the hydantoin moiety in terms of different resonance structures (Figure 4), with the nitrogen atoms exhibiting a positive π charge and the oxygen atoms bearing a negative π charge. The most positively charged nitrogen atom was found to be that showing a positive charge in a larger number of mesomeric structures (structures III and IV in Figure 4), while the relative π charges of the oxygen atoms are also in agreement with the relative number of resonance structures where these atoms appear negatively charged. On the other hand, the results also showed that the polarization of the σ system follows the inverse trends compared to those characterizing the π system. For the carbonyl groups, a higher π bond polarization towards oxygen leads to reduce the trend for the associated σ bond to be polarized in the same direction, and the same applies to the relative polarization of the π and σ systems associated with the carbon-nitrogen bonds.

Orbital interactions obtained from the NBO analyses are also in good agreement with the picture obtained based on both the geometrical parameters and the atomic charges [26-28], and the same applies when relevant parameters extracted from the AIM analysis for electron distribution characterization are taken into account. For example, a direct correlation between the value of the charge density at the bond critical points of the five bonds of the hydantoin ring in **1MH** and the corresponding bond lengths was found to exist, the shorter the bond, the greater the charge density at the associated bond critical point [27].

On the whole, the charge density analyses reveal that the main electronic effects in the hydantoin ring are, by one side, the N-to-O π electron donation, and, by the other side, the σ system back donation from the σ lone electron pairs of the oxygen atoms to the ring.

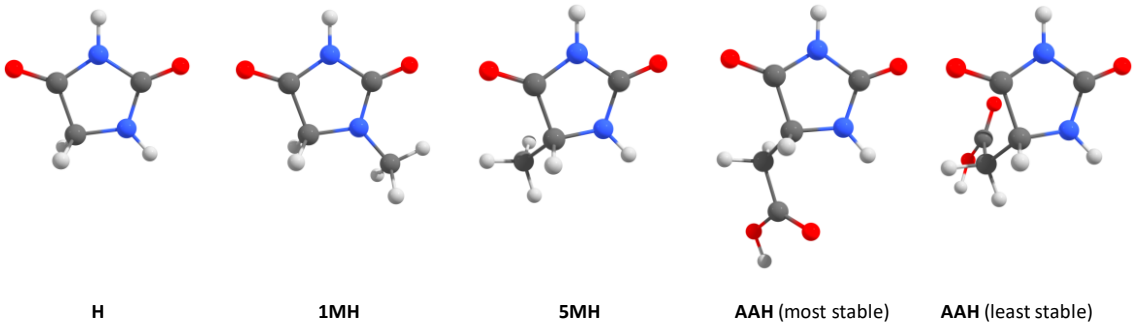

Fig. 3. Representation of the studied hydantoin molecules.

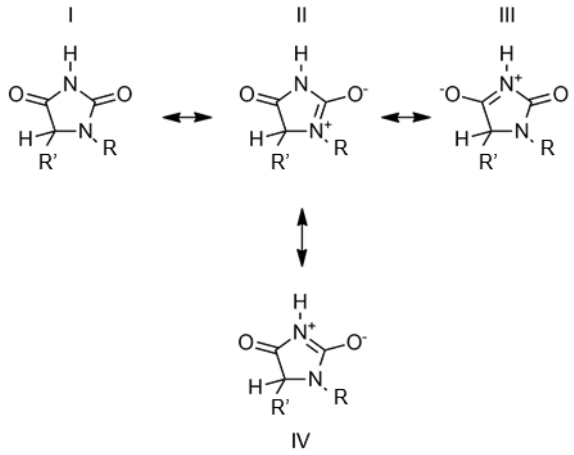

Fig. 4. I: Dominant canonic form of the hydantoin ring. II, III and IV: Mesomeric structures assuming delocalization of π electrons in the NCO fragments. R,R'= H,H (**H**); CH_3,H (**1MH**); H,CH_3 (**5MH**); H,CH_2COOH (**AAH**).

The infrared spectra of the investigated hydantoins isolated in argon matrices were found to fit well the predicted infrared spectra for the calculated minimum energy structures (see example in Figure 5, concerning **1MH**). For **AAH**, the analysis of the experimental spectrum revealed that only the most stable conformer of the molecule subsists in the matrix upon deposition. According to the calculated relative conformational energies, the room temperature gas phase population of the most stable **AAH** conformer prior to matrix deposition should be ~93%. The predicted room temperature gas phase populations for all other conformers but the second more stable one are smaller than 0.8%, *i.e.*, below the detection limit of the experimental technique; that of the second more stable conformer is ~6%, and in principle large enough to allow for its experimental detection. However, the energy barrier separating this form from the most stable conformer is very small (*ca.* 5 kJ mol^{-1}) and, under these conditions, it shall promptly convert to the lowest energy conformer during matrix deposition. Indeed, conformational cooling leading to conversion, at the time of matrix deposition, of higher-energy conformers into lower-energy forms from which they are separated by small energy barriers (of a few kJ mol^{-1}) is a well-known common phenomenon [31,32].

Detailed assignments for the matrix isolation spectra of the studied hydantoins can be found in Refs. [26-28].

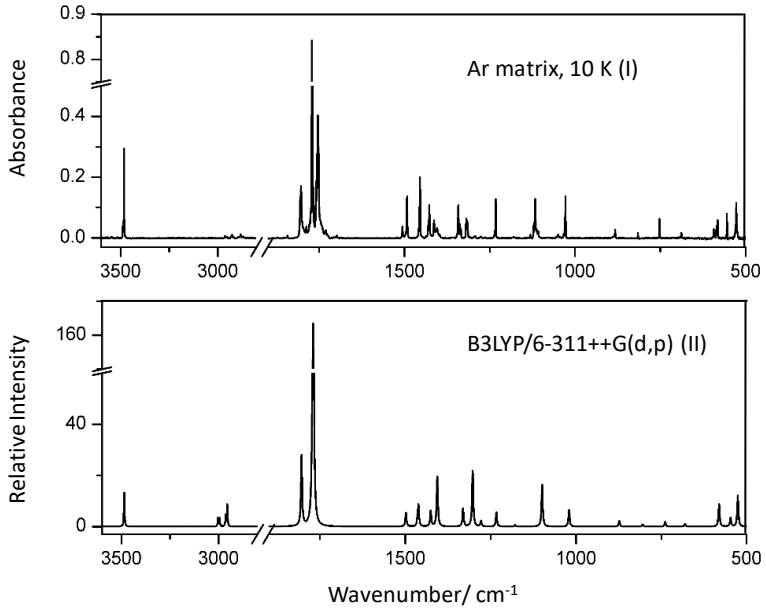

Fig. 5. Experimental infrared spectrum of monomeric **1MH** isolated in an argon matrix at 10 K (I; *top*) and B3LYP/6-311++G(d,p) calculated spectrum (wavenumbers scaled by 0.978) (II; *bottom*).

3. Photochemistry for the matrix-isolated molecules

3.1. *Mercaptoimidazoles*

The matrix-isolated thione tautomers of the studied mercaptoimidazoles were irradiated with narrowband ultraviolet (UV) light provided by a tunable Laser/MOPO system. The chosen UV wavelengths (261 nm, in the case of **MTI**, and 307 nm for both **TBI** and **MTBI**) were selected taking into account the absorption spectra of the compounds in ethanol, the time-dependent DFT (TD-DFT) calculated UV spectra for the two tautomeric forms of the compounds, as well as literature data for similar compounds [11,12,33,34].

In result of the performed irradiations, the thione tautomers were converted into the corresponding thiol forms (Figure 6). Subsequent irradiation of the matrices with shorter wavelength UV light (246 nm) successfully converted the previously generated thiol tautomers of both benzosubstituted molecules (**TBI**, **MTBI**) back to the corresponding thione forms (see Figure 6). On the other hand, the thiol→thione photochemical back-conversion could not be induced for **MTI**, upon irradiation with UV-light of wavelengths ≥230 nm.

On the whole, the experimental results clearly demonstrate that the two tautomers of the benzosubstituted mercaptoimidazoles can be photochemically interconverted in a selective way, with appropriate choice of the excitation wavelength, *i.e.*, the populations of the two tautomers can be optically controlled in an efficient manner through UV-driven reactions taking place under different excitation conditions. Another important observation is that both tautomers were found to show great stability regarding photodecomposition (no signals of photodecomposition products could be observed in the spectra along all performed irradiation experiments), what makes these chemical systems promising candidates for acting as molecular switches.

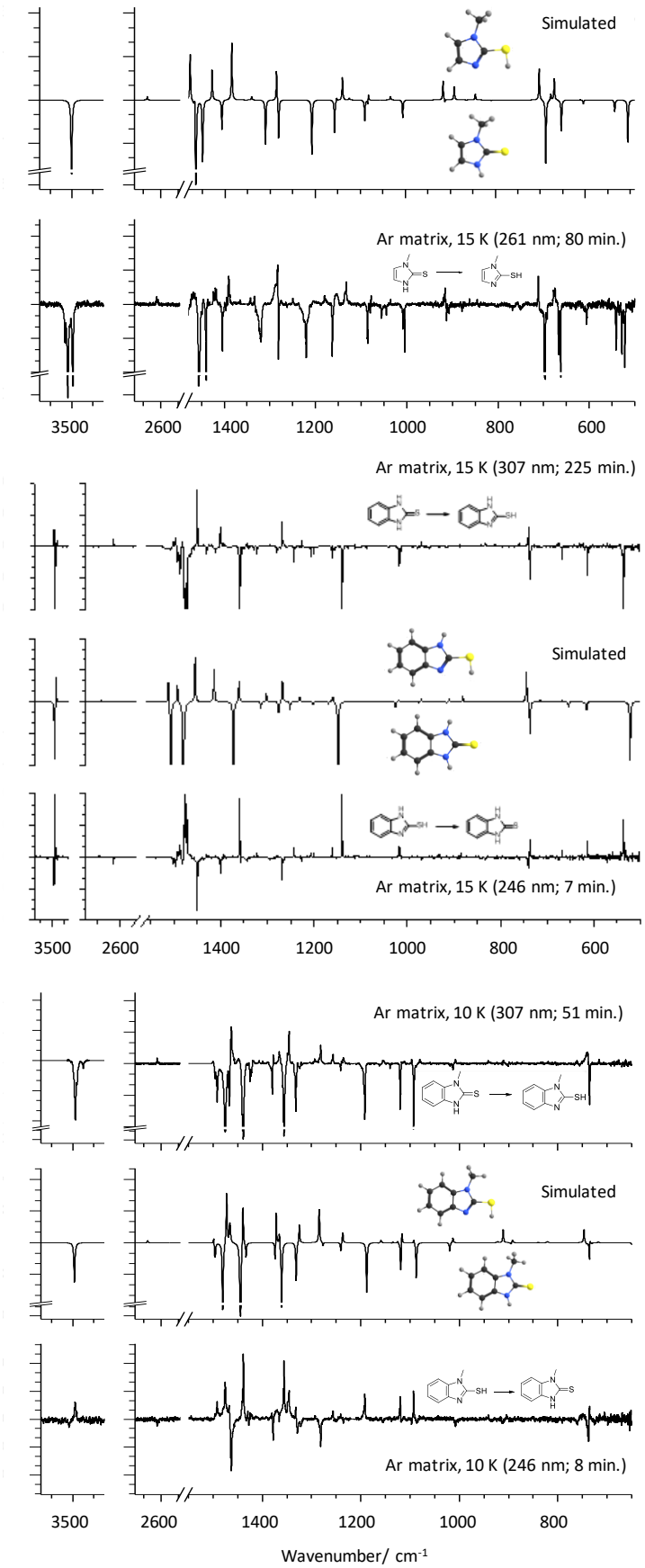

Fig. 6. Results of UV irradiations giving rise to tautomerization reactions in **MTI** (*top*), **TBI** (*middle*) and **MTBI** (*bottom*). Simulated difference spectra of the relevant species are shown for comparison.

The observed tautomeric reactions could be rationalized in terms of the PhotoInduced Detachment Association mechanism (PIDA), first proposed in the theoretical studies of Sobolewski and co-workers [35]. This mechanism involves the hydrogen photodetachment and subsequent recombination of the radical species formed upon excitation. According to the PIDA mechanism, the thiyl radical are the common intermediate species in the thione→thiol and thiol→thione phototautomerizations. Absorption of the UV light photons takes the reactant species to an excited state of (n/π)π* type, with subsequent internal conversion to a singlet state of (n/π)σ* type, leading to dissociation though cleavage of the NH or SH bonds, thus generating a hydrogen atom and the corresponding thiyl radical. The recombination of these might lead to the original species or attachment of the H atom to the S atom or N atom (depending if one is considering the thione→thiol or the inverse process) yielding the corresponding photoproduct.

After formation of the intermediate radical, its subsequent recombination with the H atom to form the final products can be expected to follow a product branch that should depend essentially on the relative stability of the products, which favors the thione tautomer and justifies the observed higher efficiency of the thiol→thione process compared to the thione→thiol isomerization. Note also that results of DFT calculations plenty support the proposed mechanism, since for both direct and reverse tautomerizations the energy of the radical-pair stays below the excitation energies. For example, in the case of **TBI** [12], for the thione→thiol isomerization E[(radical + H) – thione] = 381 kJ mol^{-1} and the used excitation wavelength was 307 nm, *i.e.*, 390 kJ mol^{-1}, whereas for the thiol→thione isomerization E[(radical + H) – thiol] = 325 kJ mol^{-1} and the used excitation wavelength was 246 nm, *i.e.*, 486 kJ mol^{-1}.

The fact that for **MTI** the photoinduced conversion of the thiol tautomer into the thione form could not be observed is also in agreement with the involvement of the thiyl radical in the photochemical process and the PIDA mechanism. Indeed, while for **TBI** and **MTBI** the intermediate radicals were shown to have a significant spin density associated with the unpaired electron in both N and S atoms, in the case of **MTI** the calculated spin density associated with the unpaired electron in the corresponding thiyl radical is practically localized only in the sulfur atom, thus making more difficult, for this molecule, recombination of the H atom at the N position. An additional factor might also contribute to the inefficiency of the thiol→thione tautomerization in **MTI**: the required excitation wavelength to induce the hydrogen atom release in **MTI** is shorter, so that larger energies must be applied to the molecule; this leads to photodecomposition to take place, as testified by observation of bands ascribable to photofragmentation products, in particular N-vinylidenemethanamine [which shall be formed together with isothiocyanic acid (SCNH) or thiocyanic acid (NCSH)] [12].

3.2. *Hydantoins*

The matrix isolated hydantoins were subjected to UV irradiations in a similar way to what has been described in the previous section for the mercaptoimidazoles. For these compounds, no tautomerization reactions were observed. On the other hand, the compounds were found to undergo fragmentation, following a common pattern of reactivity. The common photoproducts are isocyanic acid (OCNH) and CO, the first molecule being produced by cleavage of the weakest (longest) hydantoin C–C and N–C

ring bonds, as represented in Figure 7. The process occurs, with all probability, through a concerted mechanism, the third photoproduct being an imine whose precise structure depends on the reactant molecule. Illustrative spectral data showing the generation of the products of photofragmentation of **5MH** is depicted in Figure 8.

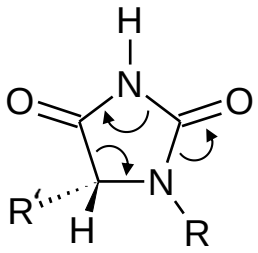

Fig. 7. Schematic representation of the concerted mechanism for the common photofragmentation of the studied hydantoins. R,R'= H,H (**H**); CH_3,H (**1MH**); H,CH_3 (**5MH**); H,CH_2COOH (**AAH**).

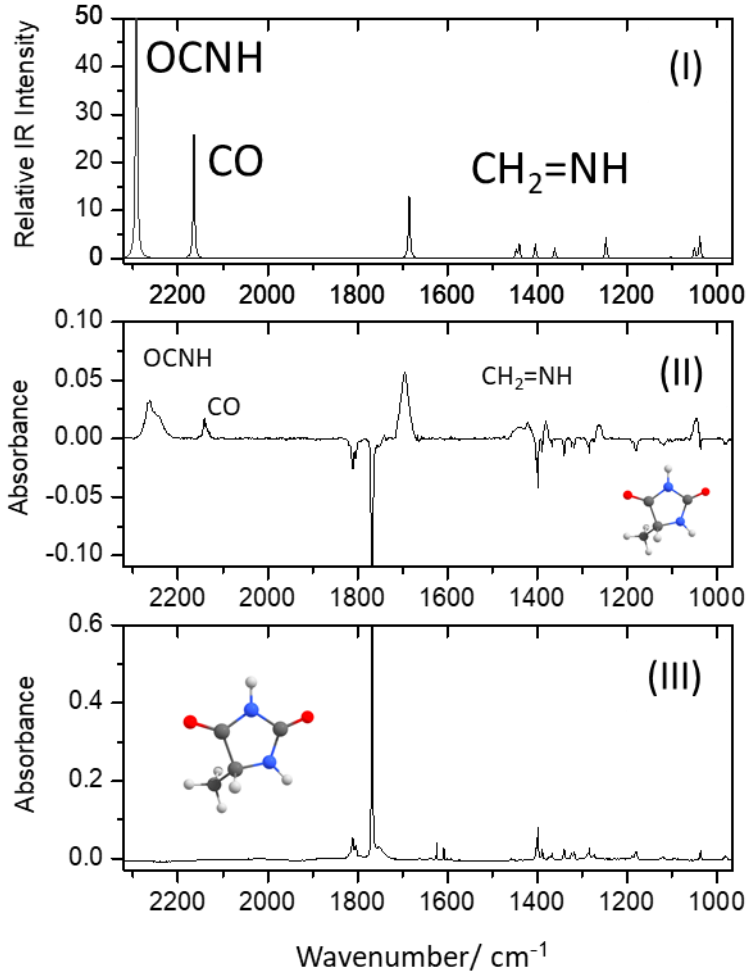

Fig. 8. B3LYP/6-311++G(d,p) calculated (scaled) infrared spectra (2320-965 cm^{-1} region) for isocyanic acid, CO and methanimine (*top*; I), infrared difference spectrum (irradiated matrix) *minus* (as-deposited) (*middle*, II), and spectrum of the as-deposited **5MH** in argon matrix (*bottom*; III).

4. Neat condensed phases – polymorphism and phase transitions

4.1. *Mercaptoimidazoles: the case of the thioimidazole dimer*

Thioimidazole undergoes easy dimerization upon crystallization from tetrahydrofuran (THF) solution, which results in production of the disulfide derivative {(2-[(1*H*-imidazol-2-yl) disulfanyl]-1*H*-imidazole]; **IDI**}. Suitable crystals for single crystal XRD experiments were collected and their structure was solved. Very interestingly, the material was found to constitute a new polymorph of the compound, which, as described below, presents unique structural features.

The structure of a crystalline phase of **IDI** had been reported previously by Bazargani and co-workers [36]. That polymorph (**I**) crystallizes in the monoclinic space group *C2/c*, with a = 14.083(3) Å, b = 6.3928(13) Å, c = 9.922(2) Å and β = 122.29(3)º, with 4 molecules per unit cell (Z = 4). The asymmetric unit of the crystals of polymorph **I** contains one half-molecule (Z' = ½). The S–S bond distance is 2.0713(14) Å, the planar imidazole rings form an angle between them of 21.83(19)º, and the C–S–S–C torsion angle is 83.62(17)º, with the two hydrogen atoms connected to the ring nitrogen atoms pointing to opposite directions. Intermolecular N–H···S hydrogen bonds result in the formation of linear chains along the *c*-direction; further $c_g \cdots c_g$ interactions between the imidazole rings of adjacent chains in the *a*-direction ($c_g \cdots c_g$ distance: 3.4466(19) Å) define the supramolecular structure in the crystal.

The structure of the newly synthesized polymorph (**II**) was found to be considerably more complex. The crystals of polymorph **II** belong to the non-centrosymmetric *Ia* monoclinic space group, with Z = 16 and cell parameters: a = 7.45910(10) Å, b = 44.1680(8) Å, c = 11.3522(2) Å and β = 103.0240(10)º. The crystals belong to the rare category of crystals having an asymmetric unit with $Z' > 1$ (only about 9% of the *ca.* 800,000 structures contained in the Cambridge Structural Database share this feature [37]). In the present case, the unit cell contains 4 symmetry independent molecules. However, the most fascinating structural feature of this new polymorph is that the symmetry independent molecules exhaust the whole set of conformers of the molecule: the abundant lowest energy conformer, and two high-energy forms not present in solution before crystallization.

The four **IDI** independent molecules present in the crystal of polymorph **II** (extracted from the XRD data; **A**-**D**), together with the calculated conformers of the molecule (**1**-**3**) are shown in Figure 9. The calculated relative energies for the different conformers as isolated species, obtained at the B3LYP/6-311++G(d,p) level of theory, are also given in the figure, as well as the C–S–S–C dihedral angles of all represented structures. In the crystal, two molecules (**C**, **D**) are similar to conformer **1**, and the remaining two, **A** and **B**, correspond to conformers **3** and **2**, respectively.

Taking into account the relative energies of the **IDI** conformers (see Figure 9), the isolated **IDI** molecule exists almost exclusively in conformer **1**, both in gas phase and solution (the energies shown in Figure 9 correspond to gas phase data; in THF, the calculated relative energies for conformers **2** and **3** are 9.7 and 9.3 kJ mol^{-1}, respectively). The most stable **IDI** conformer exhibits an intramolecular H-bond interaction established between the unprotonated nitrogen atom of one of the imidazole rings and the NH fragment of the second imidazole ring of the molecule. Because of this interaction, in conformer **1** the number of positions readily available for establishing intermolecular H-bonds is reduced to half, when compared with the higher energy conformers. Indeed, to

fulfill the four H-bond valences with intermolecular H-bonds in the crystal, the most stable **IDI** conformer has to break the intramolecular H-bond. This fact makes the energetic balance associated with the establishment of the intermolecular H-bonds less favorable for conformer **1** than for both conformers **2** and **3**, which require only minor structural rearrangements to establish intermolecular H-bonds.

It can then be concluded that the simultaneous observation of the three conformers of **IDI** in polymorph **II** results from a compromise between the greater intrinsic stability of the isolated conformer **1**, and the easier and more efficient in energetic terms packing achieved by the higher energy conformers **2** and **3**. In polymorph **I**, the **IDI** molecules assume a geometry similar to that of conformer **2**.

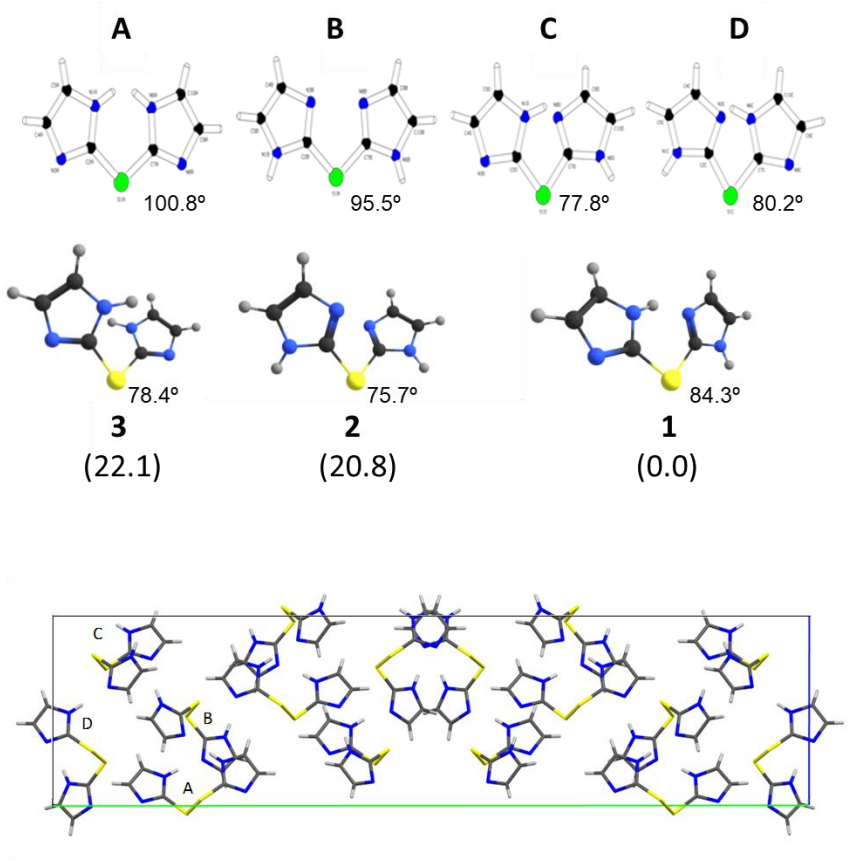

Fig. 9. Structures of the four non-equivalent molecules of **IDI** in the crystal of polymorph **II** (*top*), and equilibrium geometries for the three conformers of the isolated **IDI** molecule (*middle*). The C–S–S–C dihedral angles are indicated near each structure, and relative energies (in kJ mol^{-1}) are provided within parentheses for the calculated conformers. The *bottom* image corresponds to the XRD determined unit cell (viewed along the *a* axis), with the four molecules constituting the asymmetric unit labeled according to the names given here to each one of the non-symmetrically equivalent units in the crystal.

The Raman spectrum (500-50 cm^{-1} region) of polymorph **II** is shown in Figure 10, where it is compared with the simulated spectrum built based on the calculated Raman spectra for the three conformers of **IDI**, summed according to the relative abundance of the conformers in the crystalline state. As seen in the figure, these two spectra show a very good agreement, indicating that the intermolecular potential in the crystalline phase does not affect too much the intramolecular potentials, and also that the intermolecular

hydrogen bonds involving conformer **1** in the crystal are comparable in strength to the intramolecular hydrogen bond existing in the isolated molecule. The strong overlapping doublet of bands observed at 331/326 cm^{-1} is characteristic of the ν(S–S) stretching vibration, and its frequency is well reproduced by the calculations (scaled value).

Figure 10 shows also the calculated Raman spectrum of conformer **2**, which is the one existing in polymorph **I**, for which the experimental spectrum has not yet been reported. Assuming that the predicted spectrum of **2** would also fit properly the experimental spectrum of polymorph **I**, one can expect that the spectrum of that polymorph could be easily distinguishable from that of polymorph **II** by direct comparison of the spectral region shown in the figure. For example, the doublets observed in the Raman spectrum of polymorph **II** at 176/167, 226/222, 240/236 cm^{-1} and the overlapped doublet at 331/326 cm^{-1} can be expected to be replaced by single bands at nearly the same frequencies in the Raman spectrum of polymorph **I**. Ongoing studies will allow us to confirm these predictions.

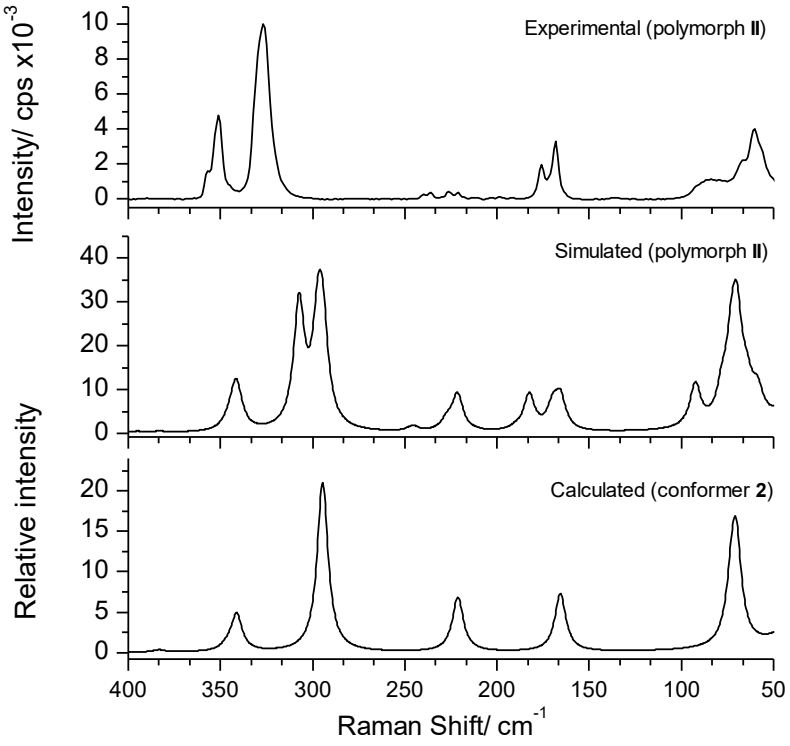

Fig. 10. Room temperature Raman spectrum of polymorph **II** of **IDI** (*top*), simulated Raman spectrum of polymorph **II** obtained by adding the calculated spectra of conformers **1**, **2** and **3**, in a ratio 2:1:1 (*middle*), and calculated spectrum of conformer **2** (the one existing in the polymorph **I** of the compound; *bottom*). Calculated spectra were scaled by 0.71.

4.2. *Hydantoins: polymorphism in **1MH** and **5MH***

The study of neat **1MH** and **5MH**, by combined use of DSC, PLTM, and infrared and Raman spectroscopies, allowed to identify several new polymorphs of these compounds, characterize them structurally, and shed light on the energetics and other relevant features of the observed phase transitions [27-29].

For **1MH**, two polymorphs were identified. Polymorph **I** was obtained by crystallization of the low temperature amorphous phase produced from fast condensation of the vapor of the compound, as well as from crystallization of most of the solvents used during the polymorph screening work. Polymorph **II** was obtained by sublimation, and by crystallization from methanol. This last polymorph converts into polymorph **I** upon warming, in a low energy solid-solid transition which takes place from about 110 to 135 ºC. The so formed polymorph **I** then melts at a temperature of 155.7 ± 0.7 ºC with an enthalpy of fusion of 21.5 ± 0.3 kJ mol^{-1}. The crystals of polymorph **I** are monoclinic, $P2_1/c$, with $Z = 4$, $a = 5.601(10)$ Å, $b = 12.178(3)$ Å, $c = 8.090(2)$ Å, $\alpha = \gamma = 90^o$ and $\beta = 105.62(2)^o$ [27]. The most relevant pattern of hydrogen bonds noticeable in the crystal of polymorph **I** is the centrosymmetric ring formed by N–H···O hydrogen bond interactions, which group **1MH** molecules in dimeric units. In turn, polymorph **II** is orthorhombic, $Pna2_1$ space group, with Z = 4, $a = 19.0258(4)$ Å, $b = 3.91210(10)$ Å and $c = 6.82880(10)$ Å [29]. The striking difference between the H-bond network in the two polymorphs is that, while in polymorph **I** the N–H···O interactions group the molecules in dimers (which are then associated by C–H···O weak interactions), in polymorph **II** the N–H···O interactions are used to form zigzag chains, which are interspersed with other chains through the interactions involving oxygen atoms and form an angle of *ca.* 36° between them [29].

In the case of **5MH**, four polymorphs were identified. Polymorph **I** corresponds to the commercial sample, which could be transformed into the remaining forms (**II**-**IV**) by thermal treatment. The melting points of the polymorphs (following their numbering) were found to be 147.2 ± 0.6, 143.0 ± 0.4, 120.1 ± 0.8 and *ca.* 94-96 ºC [28]. Only the structure of polymorph **III** could be solved by XRD, which resulted to be triclinic, *P*-1 space group, with $Z = 2$, $a = 4.3618(2)$ Å, $b = 6.1535(2)$ Å, $c = 10.3145(5)$ Å, $\alpha = 76.196(2)^o$, $\beta = 80.860(3)^o$ and $\gamma = 84.904(3)^o$ [28]. In this crystal, the molecules are packed in layers, where the molecules are joined in infinite chains through a head-to-tail pattern of hydrogen bonding involving the C=O and NH groups.

The different polymorphs of the two compounds were investigated by infrared and Raman spectroscopies.

In the case of **1MH**, analysis of the H-bond sensitive regions of the infrared spectra of the two polymorphs, allowed to estimate the average energy per H-bond in each polymorph. This was achieved by use of Rozenberg and co-workers' empirical correlations [38,39], which relate the frequency red-shifts of the stretching vibrations and/or the frequency blue-shifts of the out-of-plane bending modes of the H-bond donors (compared to the corresponding frequencies for the free groups; matrix isolation data was used as reference) with H-bond properties, including energies. The results indicate that slightly stronger N-H bonds exist in polymorph **I** than in polymorph **II** ($\Delta H_{(H\text{-}bond)} = -28$ and -26 kJ mol^{-1}, respectively). These results are in agreement with the structural crystallographic data, which indicate that the N–H bond lengths are longer and both the N···O and H···O distances associated with the N–H···O dominant intermolecular interactions are shorter in polymorph **I** than in polymorph **II**.

A very interesting result was obtained by following the transformation of a single crystal of polymorph **II** of **1MH** into polymorph **I**, by temperature variation Raman microspectroscopy. As shown in Figure 11, upon heating, the crystal of polymorph **II** converts into polymorph **I** in a transformation that kept crystal integrity [29].

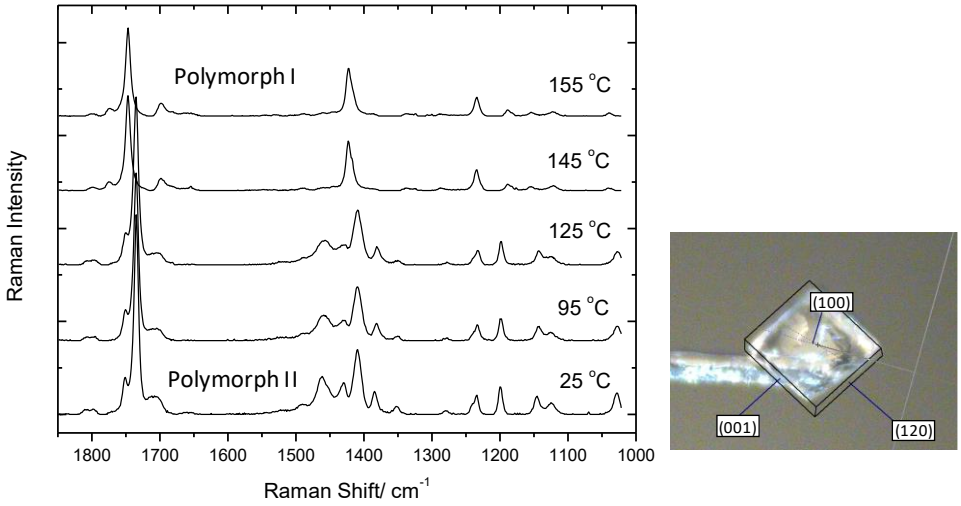

Fig. 11. (*Left*): Raman spectra of a single crystal of **1MH** (1000-1850 cm^{-1} spectral region) showing the transformation of polymorph **II** into polymorph **I**, upon heating. Spectra are obtained without polarization analyzer, *i.e.*, for the reactant polymorph the spectrum corresponds to the X(Z[YZ]$\overline{X}$) spectrum. (*Right*): Single crystal of polymorph **II** used in the Raman measurements. The Miller indices of the planes corresponding to the faces of the crystals are indicated in the figure; the laser beam (X direction) was focused on the upper faces of the crystals, and the spectra collected at 180º scattering geometry ($\overline{X}$); the crystal was sampled with the planes defining their side faces approximated aligned along the Y and Z directions.

For **5MH**, the Raman spectra of polymorphs **I** and **II** were found to be almost identical (Figure 12), except in relation to relative band intensities, indicating that that the orientation of the **5MH** molecules in both crystals shall be very similar. On the other hand, the Raman spectrum of polymorph **III** is clearly distinctive from those of polymorphs **I** and **II**, suggesting a significant dissimilarity in the H-bond network of polymorph **III** compared to those of polymorphs **I** and **II** (no Raman spectrum could be obtained for polymorph **IV**, which was found to be very labile, promptly converting to other polymorphs).

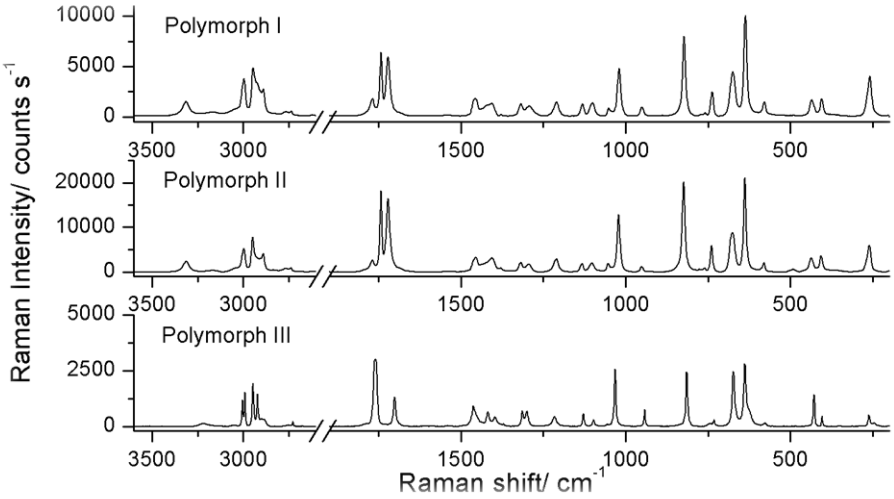

Fig. 12. Raman spectra of polymorphs **I**-**III** of **5MH**.

4.3. *Hydantoins: the unusual conformational selection in **AAH** upon crystallization*

Several polymorphs were also identified for **AAH**, which could be characterized by DSC, PLTM, Raman spectroscopy and XRD. Polymorph **I** corresponds to the commercial sample used, while the remaining polymorphs (**II**-**V**) were obtained by recrystallizations from different solvents. The melting points of polymorphs **I**, **II**, **III** and **V** were found to be 214.3 ± 0.8, 184-185, 175-178 and 198-200 ºC, respectively. Polymorph **IV** transforms into **V** at 180-185 ºC. Until now, only in the case of polymorph **III** suitable crystals could be produced for single crystal structure determination. The crystal was found to be orthorhombic, $P2_12_12_1$ space group, $Z = 4$, $a = 7.6148(5)$ Å, $b = 8.5592(6)$ Å and $c = 9.3406(6)$ Å. The molecules form chains interconnected by H-bonds (N–H···OH), which define parallel sheets of molecules.

Very interestingly, the molecules in the crystal assume the conformation of the highest energy form predicted for the isolated molecule situation (see Figure 4), which has a predicted relative energy of *ca.* 40 kJ mol^{-1}. Considering that **AAH** has 13 conformers, it is impressive that the highest energy form is the one present in the crystal. It is relatively frequent that crystallization takes place with selection of conformers that are not the lowest energy form of the isolated molecule. However, the selection of the most energetic among 13 conformers, with a relative energy as high as 40 kJ mol^{-1} is, certainly, a very rare case, implying a strongly favorable packing of the molecules in the crystal that can overcome the intrinsic unfavorable energetic requirements of the selected constituting unit. The Raman spectroscopy data obtained for the different **AAH** polymorphs is in agreement with this conclusion. In fact, the spectra of the polymorphs (Figure 13) exhibit notorious differences, which are compatible with substantially different crystal structures that, in turn, can be correlated with existence of strong intermolecular interactions and specific packing requisites. The accentuated dissimilarity between the Raman spectra of the different polymorphs may also indicate that the conformation(s) assumed by the individual molecules in each polymorph might be different. Confirmation of this hypothesis requires the determination of the crystal structure of the various polymorphs. Studies are on the way to achieve this goal.

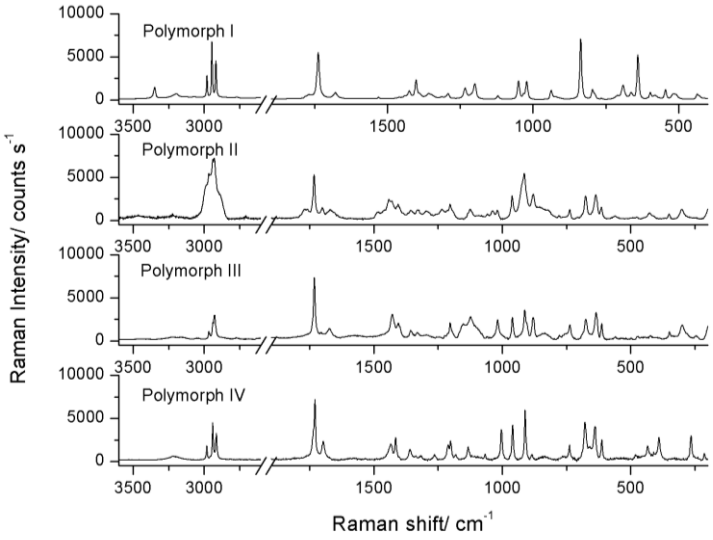

Fig. 13. Raman spectra of the polymorphs **I**-**IV** of AAH.

5. Conclusion

Modern vibrational spectroscopies play a central role in the investigation of the structure and reactivity of chemical systems, from isolated molecules to complex condensed phase structures. When used together with complementary techniques, such as XRD, DSC, PLTM, and contemporary theoretical approaches, they allow for elucidation of subtle structural details of the systems under investigation, and successfully extract fundamental information on the chemical transformations they undergo, either induced by light or thermally.

This Chapter intended to demonstrate some of the capabilities of vibrational spectroscopy as major research tool to investigate the structure and reactivity of two relevant closely-related families of nitrogen-containing heterocyclic molecules: hydantoins, and mercaptoimidazoles. Infrared spectroscopy, used in connection with the matrix isolation technique and a set of complementary computational approaches, allowed to characterize in details the structures of the isolated molecules of the compounds selected for investigation, and their photochemistry. Infrared and Raman spectroscopies, supplemented by thermodynamics, microscopy and diffraction techniques, were used to investigate neat condensed phases of the compounds and the observed transitions between these phases.

The tautomerism in the studied mercaptoimidazoles was addressed in various perspectives, from the determination of the preferred tautomeric species present in the different phases investigated, till the photochemically induced (inter)conversion between the thione and thiol tautomers of these compounds. The crystal structure of a new polymorph of the dimer of thioimidazole was described in details by a combined use of XRD, quantum chemical calculations and Raman spectroscopy. These studies reveal a fascinating crystal architecture, where 4 non-equivalent molecules are present in the unit cell, which exhaust the existing conformers of the isolated molecule of the compound.

The electronic and geometric major features of the hydantoin moiety were described, leading to the very interesting picture of reciprocal influence of the π and σ electronic systems (through π electron charge donation from the nitrogen atoms to the carbonyl oxygens and σ back-donation from these latter to the ring), which determine the details of the geometries of the studied molecules and, ultimately, also determine their photofragmentation pattern, which takes place by cleavage of the weakest bonds in the ring and keeping intact the fragment (OCNH) constituted by the strongest (shorter) bonds of the hydantoin ring. Polymorphism shown by the hydantoins has been studied and several new polymorphs identified for **1MH**, **5MH** and **AAH**. For **1MH**, an unusual transformation between the two polymorphs of the compound which takes place in keeping crystal integrity was observed. For **AAH**, an intriguing case of conformational selection where the highest energy conformer for the isolated molecule situation (higher in energy than the most stable conformer by *ca.* 40 kJ mol^{-1}) is chosen to form a crystal was described.

Acknowledgements

This investigation has been performed within the Project PTDC/QEQ-QFI/3284/2014 – POCI-01-0145-FEDER-016617, funded by the Portuguese *"Fundação para a Ciência*

e a Tecnologia" (FCT) and FEDER/COMPETE 2020-EU. The Coimbra Chemistry Centre (CQC) is supported by FCT, through the project UI0313/QUI/2013, also co-funded by FEDER/COMPETE 2020-EU. E.M.B. and B.A.N. thank FCT for the grant CCMAR/BI/0013/2017, within Project PTDC/MAR-BIO/4132/2014, the PhD. grant SFRH/BD/129852/2017, respectively. R.F. and G.O.I. acknowledge the financial support through the project MATIS - Materiais e Tecnologias Industriais Sustentáveis (FCT and CENTRO-01-0145-FEDER-000014).

References

1. Whittle, E., Dows, D.A., and Pimentel, G.C. 1954, *J. Chem. Phys.*, 22, 1943.
2. Norman, I., and Porter, G. 1954, *Nature*, 174, 508.
3. Holler, T.P., Ruan, F., Spaltenstein, A., and Hopkins, P.B. 1989, *J. Org. Chem.*, 54, 4570.
4. Hand, C.E., and Honek, J.F. 2005, *J. Nat. Prod.*, 68, 293.
5. Zoete, V., Vezin, H., Bailly, F., Vergoten, G., Catteau, J.-P., and Bernier, J.-L. 2000, *Free Rad. Res.*, 32, 525.
6. Crépin, A., Wattier, N., Petit, S., Bischoff, L., Fruit, C., and Marsais, F. 2009, *Org. Biomol. Chem.*, 7, 128.
7. Nagasaka, A., and Hidaka, H.,1976, *J. Clin. Endocrin. & Metabol.*, 43, 152.
8. Heath, H., and Toennies, G, 1958, *Biochem. J.*, 68, 204.
9. Phan, H., Lekin, K., Winter, S.M., Oakley, R.T., and Shatruk, M. 2013, *J. Am. Chem. Soc.*, 135, 15674.
10. Matsuzaki, H., Fujita, W., Awaga, K., and Okamoto, H. 2003, *Phys. Rev. Lett.*, 91, 017403.
11. Brás, E.M., Fausto, R. 2018, *J. Mol. Struct.*, in press (doi: 10.1016/j.molstruc.2018.02.013)
12. Brás, E.M., Fausto, R. 2018, *J. Photochem. Photobiol. A: Chemistry*. In press (doi: 10.1016/j.jphotochem.2018.02.035)
13. Arunan, E., Desiraju, G.R., Klein, R.A., Sadlej, J., Scheiner, S., Alkorta, I., Clary, D.C., Crabtree, R.H., Dannenberg, J.J., Hobza, P., Kjaergaard, H.G., Legon, A.C., Mennucci, B., and Nesbitt, D.J. 2011, *Pure Appl. Chem.*, 83, 1637.
14. Lodochnikova, O.A., Bodrov, A.V., Saifina, A.F., Nikitina, L.E., and Litvinov, I.A. 2013, *J. Struct. Chem.*, 54, 140.
15. Khan, H., Badshah, A., Shaheen, F., Giek, C., and Qureshi, R.A. 2008, *Acta Cryst. E*, 64, o1141.
16. Form, G.R., Raper, E.S., and Downie, T.C. 1976, *Acta. Cryst. B*, 32, 345.
17. Block, S.S. Disinfection, Sterilization and Preservation, 4th Ed., Lea & Febiger Inc., Philadelphia, USA, 2003.
18. Kumar, C.S.A., Kavitha, C.V., Vinaya, K., Prasad, S.B.B., Thimmegowda, N.R., Chandrappa, S., Raghavan, S.C., and Rangappa, K.S. 2009, *Invest. New Drugs*, 27, 327.
19. Kavitha, C.V., Nambiar, M., Kumar, C.S.A., Choudhary, B., Muniyappa, K., Rangappa, K.S., and Raghavan, S.C. 2009, *Biochem. Pharmacol.*, 77, 348.
20. Sarges, R., Schnur, R.C., Belletire, J.L., and Peterson, M.J. 1988, *J. Med. Chem.*, 31, 230.
21. Yang, K., Tang, Y., and Iczkowski, K.A. 2010, *Am. J. Transl. Res.*, 2, 88.
22. Park, H.S., Choi, H.J., Shin, H.S., Lee, S.K., and Park, M.S. 2007, *Bull. Korean Chem. Soc.*, 28, 751.
23. Comber, R.N., Reynolds, R.C., Friedrich, J.D., Manguikian, R.A., Buckheit, R.W., Truss, J.W., Shannon, W.M., and Secrist, J.A. 1992, *J. Med. Chem.*, 35, 3567.
24. Cruz-Cabeza, A.J., and Schwalbe, C.H. 2012, *New J. Chem.*, 36, 1347.
25. Faris, W.M., and Zaki, S.S. 2014, *Orient. J. Chem.*, 30, 1045.
26. Ildiz, G.O., Nunes. C.M., and Fausto R. 2013, *J. Phys. Chem. A*, 117, 726.
27. Nogueira, B.A., Ildiz, G.O., Canotilho, J. Eusébio, M.E.S., and Fausto, R. 2014, *J. Phys. Chem. A*, 118, 5994.

28. Nogueira, B.A,, Ildiz, G.O., Canotilho, J., Eusébio, M.E.S., Henriques, M.S.C., Paixão, J.A., and Fausto, R. 2017, *J. Phys. Chem. A*, 121, 5267.
29. Nogueira, B.A., Ildiz, G.O., Henriques, M.S.C., Paixão, J.A., and Fausto, R. 2017, *J. Mol. Struct.*, 1148, 111.
30. Ildiz, G.O., Boz, I., and Unsalan, O. 2012, *Opt. & Spectrosc.*, 112, 665.
31. Rosado, M.T.S., Lopes Jesus, A.J., Reva, I.D., Fausto, R., and Redinha, J.S. 2009, *J. Phys. Chem. A*, 113, 7499.
32. Reva, I.D., Lopes de Jesus, A.J., Rosado, M.T.S., Fausto, R., Eusébio, M.E., and Redinha, J.S. 2006, *Phys. Chem. Chem. Phys.*, 8, 5339.
33. Reva, I., Nowak, M.J., Lapinski, L., and Fausto, R. 2015, *Phys. Chem. Chem. Phys.*, 17, 4888.
34. Rostkowska, H., Lapinski, L., Khvorostov, A., and Nowak, M.J. 2003, *J. Phys. Chem. A*, 107, 6373.
35. Chmura, B., Rode, M.F., Sobolewski, A.J., Lapinski, L., and Nowak, M.J. 2008, *J. Phys. Chem. A*, 112, 13655.
36. Bazargani, M.F., Talavat, L., Naderi, S., and Khavasi, H.R. 2011, *Acta Cryst. E*, 67, o2585.
37. Steed, K.M., and Steed, J.W. 2015, *Chem. Rev.*, 115, 2895.
38. Rozenberg, M.S. 1996, *Spectrochim. Acta A*, 52, 1559.
39. Rozenberg, M.S., Shoham, G., Reva, I., and Fausto, R. 2004, *Spectrochim. Acta A*, 60, 463.